J. Microelectron. Manuf. **3**, 20030407 (2020)
doi: 10.33079/jomm.20030407

Nano-Electronic Simulation Software (NESS): A Novel Open-Source TCAD Simulation Environment

Cristina Medina-Bailon [*], Tapas Dutta, Fikru Adamu-Lema, Ali Rezaei, Daniel Nagy,

Vihar P. Georgiev[**], and Asen Asenov

Device Modelling Group, James Watt School of Engineering, University of Glasgow, G12 8LT Glasgow, UK.

Abstract: This paper presents the latest status of the open source advanced TCAD simulator called Nano-Electronic Simulation Software (NESS) which is currently under development at the Device Modeling Group of the University of Glasgow. NESS is designed with the main aim to provide an open, flexible, and easy to use simulation environment where users are able not only to perform numerical simulations but also to develop and implement new simulation methods and models. Currently, NESS is organized into two main components: the structure generator and a collection of different numerical solvers; which are linked to supporting components such as an effective mass extractor and materials database. This paper gives a brief overview of each of the components by describing their main capabilities, structure, and theory behind each one of them. Moreover, to illustrate the capabilities of each component, here we have given examples considering various device structures, architectures, materials, etc. at multiple simulation conditions. We expect that NESS will prove to be a great tool for both conventional as well as exploratory device research programs and projects.

Keywords: Integrated Simulation Environment, Variability, Drift-Diffusion, Quantum Correction, Kubo-Greenwood, Non-Equilibrium Green's Function.

1. Introduction

Two of the major issues with experimental research and design are cost and time. Technology computer-aided design (TCAD) plays a crucial role in reducing the development costs and time-to-market for the semiconductor industry by performing physical analysis of already existing devices or novel technologies and transistor architectures [1]. Therefore, in the development of the TCAD tools, there are two key objectives: accurate physical models and reduced simulation time.

A great amount of commercially available TCAD software [2,3] as well as academic simulation tools with different levels of complexity, including drift-diffusion (DD) with quantum corrections [4,5], 3D ensemble Monte Carlo (MC) [6-8], multi-subband (MS) 2D [9] and 1D MC [10], direct Boltzmann Transport Equation (BTE) solvers [11], Non-Equilibrium Green's Function (NEGF) simulators in ballistic regime [12] and with scattering [13] already exist. However, the commercial TCAD tools so far are not open source software, which limits collaboration. Meanwhile, the academic software tends to work in isolation, and it is difficult to investigate a particular transistor structure with different complexity of simulation techniques [14].

In this paper, we introduce the concepts and the inner workings of a user-friendly and open-source TCAD semiconductor device simulator called Nano-Electronic Simulation Software (NESS), developed by the Device Modelling Group at the University of Glasgow. NESS enables simulations, with increasing complexity and physical content within a unified environment. Open source also means that it allows collaboration and co-development by industry and academia all over the world. NESS is designed to be flexible, easy to use, and extendable thanks to its modular structure [14].

This paper is organized as follows. In Section 2, we provide a brief overview of the NESS structure. In Section 3, we discuss the structure generator (SG) module used for the generation of the mesh and device structure which are used as an input file for rest components of NESS. Section 4 provides a detailed overview of the numerical modules already implemented: DD, Kubo-Greenwood (KG) and, NEGF. Finally, in Section 5, we finish with the concluding remarks.

[*] Address all correspondence to Cristina Medina-Bailon, E-mail: cristina.medinabailon@glasgow.ac.uk

[**] Address all correspondence to Vihar P. Georgiev, E-mail: vihar.georgiev@glasgow.ac.uk

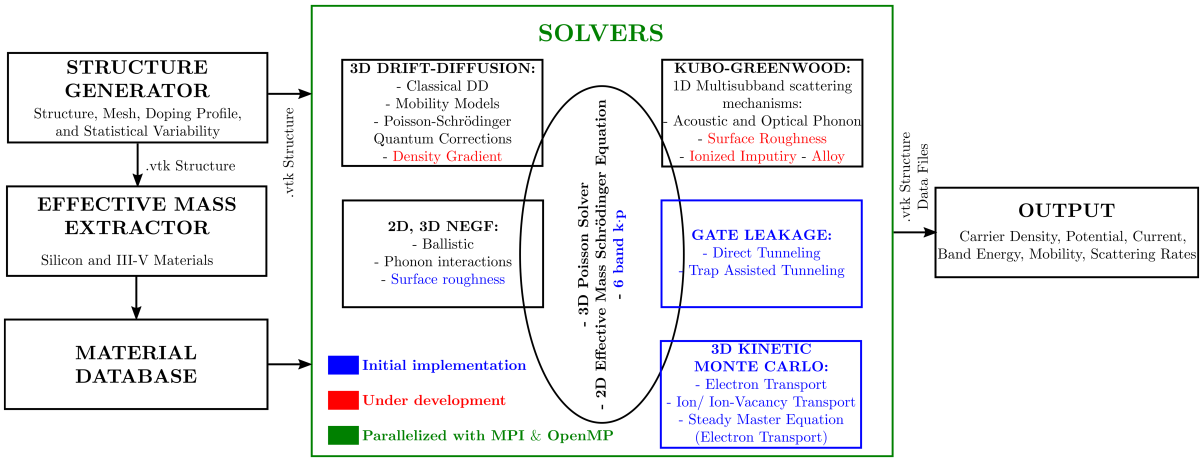

Figure 1. Flowchart of NESS detailing its modular structure.

2. Overview of NESS

In this section, we provide an overview of our simulation environment NESS and its modular structure. Currently, there are five main components of NESS which are summarized in Figure 1: SG, effective mass extractor, material database, solvers, and outputs. First, the SG [15,16] (more details in Section 3) is used to generate and configure the 3D device structures such as nanowires (NWs), multi-gate 3D device architectures, or bulk complementary metal-oxide-semiconductor (CMOS) transistors. It allows users to consider different semiconductor materials (such as Si, Ge, or III-Vs materials), doping configurations (such as uniform or Gaussian profiles), mesh designs, and the main variability sources (random discrete dopants (RDD), line edge roughness (LER), and metal gate granularity (MGG)).

Second, as the effective masses strongly depend on the confinement orientation of the nanostructures, an automated routine to extract the effective mass from first principle simulations has been implemented in NESS [1]. It can calculate the correct electron confinement and transport effective masses from atomistic simulations (such as Density Functional Theory (DFT)) or semi-empirical models (such as Tight-Binding (TB)) of the electronic band structure of NW with the technologically relevant cross-sectional area, shape, and transport orientations.

Third, the material database provides the relevant parameters for each material considered in the generated structure, such as the work-function, affinity, dielectric constants, mobility model parameters, or scattering parameters. Furthermore, the effective masses can be provided for each material from DFT and TB methods, or directly from our effective mass extractor. As illustrated in Figure 1, those parameters serve as input for the solvers.

Fourth, different transport simulation solvers [14] have been already implemented in NESS to simulate the mobility, the charge density, and the current in nano-CMOS devices. They have been implemented with a high degree of parallelism making use of MPI and OpenMP libraries. In general, each of them is self-consistently solved with the 3D Poisson and/or the 2D Schrödinger equations. Section 4 describes in details the three current main numerical solvers: *(i)* DD module, which contains different mobility models and Poisson-Schrödinger quantum corrections [17]; *(ii)* KG module, which calculates the low-field electron mobility; and *(iii)* the coupled mode-space NEGF solver, which captures quantum mechanical effects, coherent transport, and impact of scattering. Moreover, different enhanced modules and solvers [18] are currently under development in NESS including: density gradient; extension of the KG module [19] to consider surface roughness (SR), ionized impurity, and alloy scattering mechanisms; implementation of SR scattering mechanism in the existing NEGF module [20]; Kinetic MC solver [21] for the simulation of memory devices; module to compute the gate leakage current; and a full-band quantum transport solver in presence of hole-phonon interactions using a mode-space k·p approach in combination with the existing NEGF module [22].

Finally, the simulation results (i.e. current, electrostatic potential, charge concentration) are stored in text files and in vtk format for easy visualization with freeware software, such as ParaView.

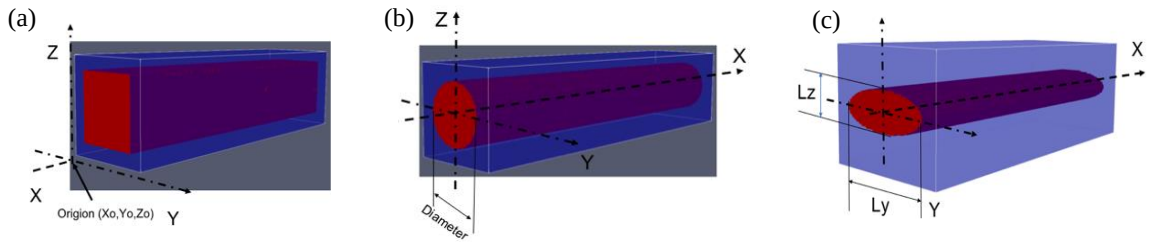

Figure 2. Some of the main primitive objects that can be used to create complex device structures.

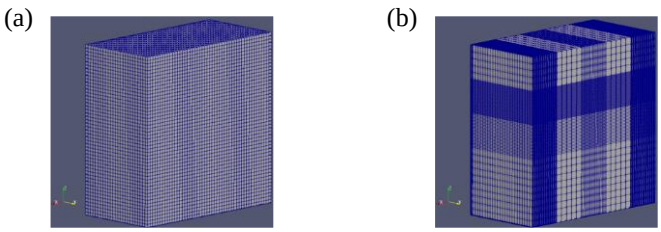

Figure 3. Uniform and non-uniform mesh generation examples.

3. Structure Generator

In this section, we introduce the device SG and provide some examples. The SG is a flexible module capable of generating various types of devices and the corresponding structures (simulation domains). The generated device structure data file can be stored as a binary or ASCII format where the datasets are defined by the rectilinear grid with a regular topology along the coordinates.

Creation of geometric objects: Users can create any type of polygon shape and three main types of geometric objects, which are (a) cuboid, (b) cylinder with circular cross-section and (c) cylinder with elliptical cross-section as shown in Figure 2. The simple elliptical shape ($z^2/l_z + y^2/l_y$) assumes that the origin is located at (0,0,0), and implemented in NESS to create both cylinder types. When assigning material and doping properties to the mesh, NESS makes two important assumptions. Materials are considered as a property of an element defined by a volume of ($\Delta V = \Delta x \cdot \Delta y \cdot \Delta z$). On the other hand, doping is assigned to a discretization node. Users can generate uniform (Figure 3(a)) and non-uniform (Figure 3(b)) meshes for their device structure.

Bulk MOSFET and SOI example: Figure 4 shows examples of conventional bulk MOSFET and fully depleted Silicon on Insulator (FDSOI) structures, generated using the NESS SG.

Statistical variability: The contemporary CMOS transistors are highly susceptible to statistical variability and their performance and electrical characteristics could be significantly affected by it. The SG can introduce the main sources of statistical variability in the device structure prior to running the simulations. In NESS, users can choose from three sources of variability: RDD [23], LER [24], and MGG [25]; or they can run simulations considering all sources of variability or different combinations of them. Figure 5 shows a randomly generated atomistic device considering RDD and MGG in the simulation domain.

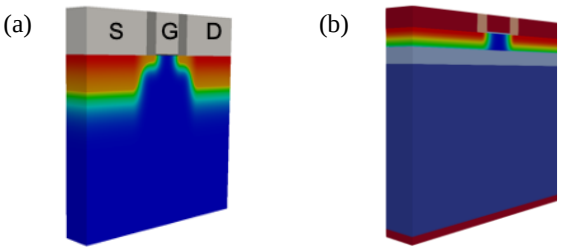

Figure 4. (a) Conventional bulk MOSFET, and (b) FDSOI.

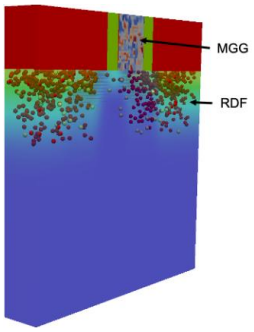

Figure 5. Atomistic device considering RDD and MGG.

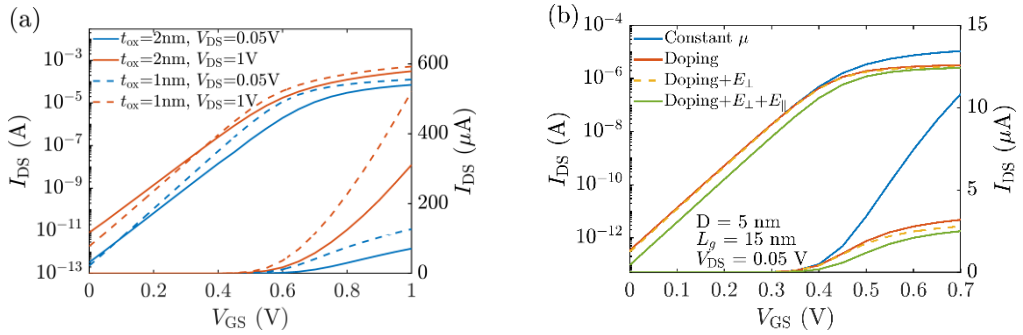

Figure 6. (a) Transfer characteristics of the bulk MOSFET shown in Figure 4(a) at low and high drain bias for t_{ox}=1nm, 2nm using DD. Constant bulk mobility of 1400 $cm^2V^{-1}s^{-1}$ was used. (b) Impact of mobility models on the transfer characteristics of a nanowire FET with circular cross section having a diameter of 5nm and channel length of 15nm, $N_{Channel}=10^{15}$ cm^{-3} and $N_{SD}=10^{20}$ cm^{-3}. The low field mobility used was 481 $cm^2V^{-1}s^{-1}$ calculated using the KG module including the impact of acoustic and optical phonon scattering mechanisms (Section 4.2).

4. Numerical Solvers

4.1 Drift-Diffusion

The DD formalism for carrier transport has been the main workhorse in the TCAD industry for many decades. It is indispensable for simulating bulk CMOS transistors and relatively larger devices where a more sophisticated approach is neither desired nor practical.

In NESS, we have implemented the DD module using a finite volume discretization scheme for the current continuity equation following the Scharfetter-Gummel approach [26] using Bernoulli functions. The 3D current continuity equation is self-consistently solved with the 3D Poisson equation until convergence. Different mobility models are included in the current continuity equation. Convergence for potential and charge is reached when the max norm of the difference between two successive Gummel iterations reaches the preset criteria. At present, we have included doping dependence of the mobility using the Masetti model [27]. The transverse and longitudinal electric field ($E_\perp$, $E_\parallel$, respectively) dependence of the mobility has been included by means of the Yamaguchi model [28] and the Caughey-Thomas [29] model, respectively. As examples, simulation results for a conventional bulk MOSFET with channel length of 25nm for two oxide thicknesses are shown in Figure 6(a), for low and high drain bias conditions considering constant bulk mobility. In Figure 6(b), we have shown the cumulative impact of the mobility models on the transfer characteristics for a nanowire transistor with a circular cross-section of 5nm diameter and 15nm channel length.

A key issue with classical DD simulations is that they cannot capture the quantum confinement effects. A quantum-corrected DD simulator can ensure a correct charge profile in the device at a fraction of the computational cost of a full quantum simulator. We have developed and implemented Schrödinger equation-based quantum-corrected DD approach in NESS [17]. For this, we first self-consistently solve the 2D Schrödinger equation in planes perpendicular to transport and 3D Poisson equation in the whole device. The 3D quantum charge is calculated using a top of the barrier approach [30], summing over all subbands and valleys. At convergence, the quantum charge density (n_Q) is used to calculate a quantum correction term $k_BT/q\log(n_Q/N_C)$ where N_C is the conduction band density of states, T is temperature, k_B is Boltzmann constant, and q is the electronic charge [31,32]. This term is then used to generate a corrected potential which (instead of the classical potential obtained from the Poisson equation) is used as a driving force in the continuity equation. This is repeated until the charge and the potential converge. The quantum correction can either be fixed for a bias point (for low drain voltage) or can be updated in each Gummel iteration. It is worthwhile to note that this approach does not use any fitting parameters in the quantum correction procedure unlike the density gradient or the effective potential method.

The quantum-corrected DD remedies the deficiency of the classical DD charge profile as can be seen in Figure 7(a) for a nanowire FET with an 5nm × 5nm square cross-section. Further, in contrast to the classical DD, current-voltage characteristics obtained using quantum-corrected DD display the shift in threshold voltage due to quantum confinement with is in an excellent match with the result obtained from ballistic NEGF as shown in Figure 7(b).

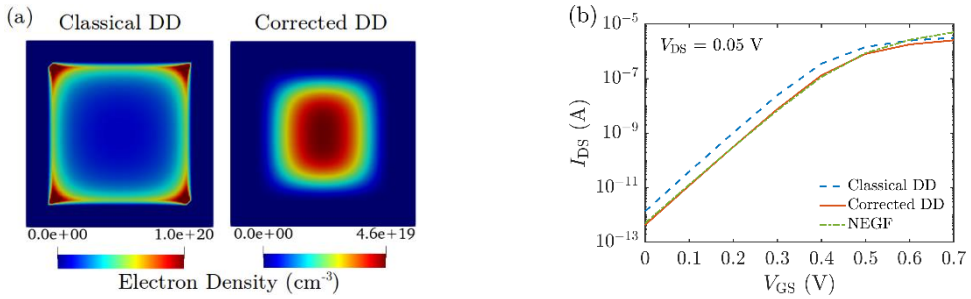

Figure 7. (a) 2D profile of electron density in a [110] oriented NW with 5nm × 5nm square cross section and L_G=10nm for classical (left) and quantum-corrected (right) DD in the plane normal to transport direction at the middle of the channel at V_{GS}=0.7V, V_{DS}=0.05V. (b) I_{DS}–V_{GS} characteristics calculated using classical DD, quantum-corrected DD, and ballistic NEGF. Note that in these simulations, in case of NEGF and for charge calculation after solving Schrödinger equation in corrected DD, the Fermi level at the source, E_{FS} is set to the quasi-Fermi level at the source contact as obtained in DD. The low field mobility used was 477 $cm^2V^{-1}s^{-1}$ calculated using the KG module.

4.2. Kubo-Greenwood Module

The KG solver implemented in NESS provides accurate electron mobility at low-field near-equilibrium conditions [33,34]. It combines the quantum effects based on the 1D multi-subband scattering rates of the most relevant scattering mechanisms in confined channels [19] and the semi-classical BTE by applying the KG formula within the relaxation time approximation [11]. In the first step, the NEGF module of NESS is used to extract the electron densities, subband levels (E_l), and the corresponding wavefunctions (ξ_l) at the cross-section area of a gated NW in the presence of a low electric field in the transport direction (the long-channel device approximation).

In the second step, the 1D rates for the dominant scattering mechanisms in silicon are calculated using the parameters from the first step. The scattering rates are directly derived from the Fermi Golden Rule, using the time-dependent perturbation theory and assuming that the transitions between two states occur instantaneously. In this paper, we present two of the implemented scattering mechanisms:

Acoustic (Ac) phonon scattering is considered to be elastic and within the short-wave vector limit. Its equivalent equation from an initial subband l and a final subband l' is:

$$\Gamma_{Ac}(l,k)=\frac{|D_{Ac}|^2 k_B T}{\rho\hbar u_s^2}\frac{m_v}{\hbar^2}\sum_{l'}\left[\int d\vec{s}\,|\xi_l(\vec{s})|^2|\xi_{l'}(\vec{s})|^2\right]\times\theta\left(\epsilon(k)+\Delta E_{l'}\right)\left(\frac{1}{|q_1+k|}+\frac{1}{|q_2+k|}\right), \quad (1)$$

where D_{Ac} is the acoustic deformation potential, ρ is the material density, $\hbar$ is the reduced Planck's constant, u_s is the speed of sound, m_l is the electron effective mass in the transport direction, $\vec{s}$ are vectors normal to the transport direction, θ represents the step function, $\epsilon(k)$ is the kinetic energy for a wavevector with magnitude k, $\Delta E_{l'}=E_{l'}-E_l$ is the energy separation between subbands l and l', and $q_{1/2}=-k\pm\sqrt{k^2+\frac{\Delta E_{l'}2m}{\hbar^2}}$.

Optical (Op) phonon scattering takes into account g-type and f-type transitions (intra- and inter-valley transitions, respectively) and the energies of the different branches of the optical deformation potential are considered constant (as used in most of the standard approaches). Accordingly, the optical phonon scattering rate for the phonon mode j can be written as:

$$\Gamma_{Op}(j,l,k)=\frac{|D_{Op,j}|^2}{2\rho\omega_j}\sum_{l'}\left[\int d\vec{s}\,|\xi_l(\vec{s})|^2|\xi_{l'}(\vec{s})|^2\right]\times\int dqG(q), \quad (2)$$

where

$$\int dqG(q)=\frac{n_j\theta\left(\epsilon(k)+\Delta E_{l'j}^{+}\right)m_{v'}}{\hbar^2}\left(\frac{1}{|q_1+k|}+\frac{1}{|q_2+k|}\right)+\frac{\left(n_j+1\right)\theta\left(\epsilon(k)+\Delta E_{l'j}^{-}\right)m_{v'}}{\hbar^2}\left(\frac{1}{|q_3+k|}+\frac{1}{|q_4+k|}\right), \quad (3)$$

with

Table 1. Main dimensions, doping values, and scattering parameters for the cylindrical Si NWs.

Device Parameters	Si width	From 3nm to 6nm	Scattering parameters	D_{Ac}	14eV
	SiO_2 width	0.8nm		$D_{Op,j}$ (g-type)	[5,8,30] $\cdot 10^9$eV/m
	Doping	10^{15}cm^{-2}		$D_{Op,j}$ (f-type)	[1.5,34,40] $\cdot 10^9$eV/m
	Temperature	300		ω_j (g-type)	[0.01206,0.01853,0.063] eV
	Effect. Mass	Ref. [1]		ω_j (f-type)	[0.01896,0.0474,0.05903] eV

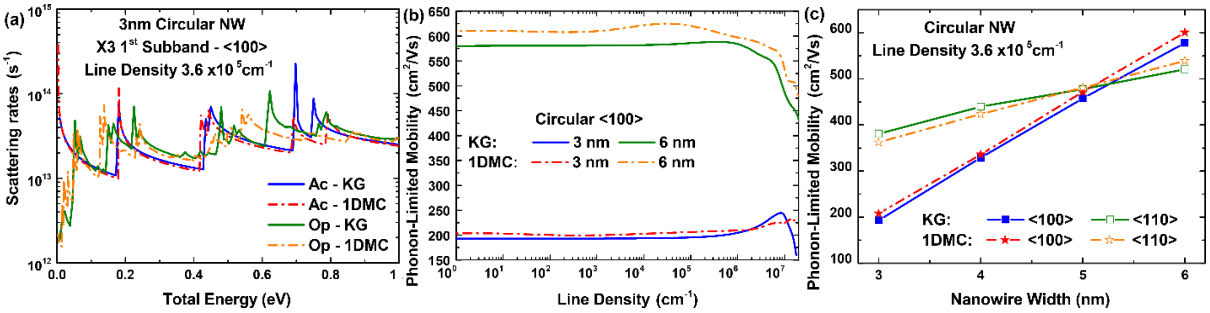

Figure 8. Scattering rates and mobility comparison between the KG module from NESS and the 1DMC code from [10]: (a) Acoustic and optical phonon scattering rates of the first subband of valley X3 as a function of the total energy for a 3nm circular NW with a line density of 3.6×10^5cm^{-1} and ⟨100⟩ orientation. (b) Phonon-limited electron mobility as a function of the line density for 3nm and 6nm circular NWs with ⟨100⟩ orientation. (c) Phonon-limited electron mobility as a function of the width for circular NWs with a line density of 3.6×10^5cm^{-1}, ⟨100⟩ and ⟨110⟩ orientations.

$$q_{1/2} = -k \pm \sqrt{\frac{m_{v'}}{m_v}k^2 + \frac{\Delta E^{+}_{l'j} 2m_{v'}}{\hbar^2}};$$

$$q_{3/4} = -k \pm \sqrt{\frac{m_{v'}}{m_v}k^2 + \frac{\Delta E^{-}_{l'j} 2m_{v'}}{\hbar^2}} \text{ and} \qquad (4)$$

$$\Delta E^{+/-}_{l'j} = E_{l'} - E_l \pm \hbar\omega_j,$$

Here, n_j is the phonon number, ω_j is the phonon energy, $D_{Op,j}$ is the optical deformation potential, and $m_v(m_{v'})$ is the transport effective mass of the initial(final) valleys, respectively.

In the third step, the mobility (μ_i^l) for the scattering mechanism i and subband l is calculated considering the semi-classical simulation of the transport properties of a 1D electron gas using the BTE within the relaxation time approximation [11] as a function of the relaxation time ($\tau_i^l(E) = 1/\Gamma_i^l(E)$), the 1D density of states (g_l), the Fermi-Dirac function (f_0), and the 1D electron concentration (N_l):

$$\mu_i^l = \frac{2q}{k_B T N_l m_l}\int dE g_l(E)\left(E - E_l\right)\tau_i^l(E) f_0(E)\left(1 - f_0(E)\right). \qquad (5)$$

In the fourth step, we calculate in two strategies the total mobility for the l subband (μ^l): *(1)* it is calculated as a function of the individual mobilities associated with each scattering mechanism (μ_i^l) using the Matthiessen rule ($1/\mu^l = \sum_i 1/\mu_i^l$); and *(2)* the scattering rates of all mechanisms are directly added to avoid the Matthiessen rule and thereby μ^l is computed using Equation (5). The former strategy is of special interest for devices with large cross sections because the error induced by the Matthiessen rule in narrower devices is comparable to MS-MC and NEGF approaches. Finally, the average mobility of a NW structure is calculated accounting for all the subbands: $\mu_{NW} = \sum_l N_l \mu^l / \sum_l N_l$. The advantage of both semi-classical alternatives in comparison to purely quantum transport simulations is that the rates are individually computed and then combined, reducing dramatically the computational cost.

Figure 8 shows the scattering rates and mobility for cylindrical Si NWs, which main parameters are summarized in Table 1. The results from the KG module have been compared to the results of an external to NESS 1DMC simulator [10], where the mobility is extracted after applying a small constant electric field by fitting the average velocity versus field dependence. In general, the 1DMC and KG scattering rates for the lowest subband of the 3nm nanowire (Figure 8(a)) are in very good agreement especially at low energy levels, the most relevant region which determines the accuracy of the low-

field mobility calculations. Moreover, the phonon-limited mobility computed with both approaches shows a very good agreement as a function of the line density (Figure 8(b)) for a 3nm and 6nm circular NW with ⟨100⟩, and as a function of the NW widths (Figure 8(c)) at a fixed line density for ⟨100⟩ and ⟨110⟩ orientations

4.3. NEGF

The so-called NEGF formalism, which is derived based on the Keldysh technique [35], is a widely applied framework for analyzing the electronic transport in non-equilibrium many-body systems. This method allows a quantum treatment of charge transport in order to capture quantum phenomena such as tunneling, coherence, and particle-particle interactions in mesoscopic and nanoscale devices. We obtain the charge density, potential profile, and the current flow in the system by performing a self-consistent solution of the Poisson equation and the NEGF transport equations in coupled-mode space (CMS). We can either consider diffusive transport by switching on the acoustic- and/or optical-phonon scattering [36,37] to enable electron-phonon (e–ph) interactions within the self-consistent Born approximation (SCBA) or neglect them to investigate merely the ballistic transport [13]. Moreover, we can simulate 2D planar structures such as DGSOI [38], and the NEGF solver implemented in NESS also allows calculation of the band-to-band tunneling by using the Flietner model to compute the current in heterostructures with a direct bandgap [39].

Adopting the notation of Reference [14], we will summarize the main concepts required to understand the NEGF formalism. Having the system in a steady state, the retarded, advanced, and lesser/greater Green's functions in real space representation read:

$$G^R(E)=\frac{1}{(E+i\eta)\cdot I-h-\Sigma^R(E)},G^A(E)=\left[G^R(E)\right]^\dagger, \tag{6}$$

$$G^{\lessgtr}=G^R(E)\cdot\Sigma^{\lessgtr}(E)\cdot G^A(E), \tag{7}$$

where, h, and $\Sigma^{R(\lessgtr)}$ represent the one-particle Hamiltonian, and the retarded (lesser/greater) self-energies accounting for electrons interactions with their surroundings, respectively. The charge at position r and the current take the forms:

$$n(r)=-\frac{i}{2\pi}\int dE\,G^<(r,r';E) \tag{8}$$

$$j(l)=\frac{2\cdot|q|}{\hbar}\int\frac{dE}{2\pi}\mathrm{Tr}\left[2\,\mathrm{Re}\left\{h_{l+1,l}\cdot G^<_{l,l+1}\right\}\right] \tag{9}$$

Here $h_{l+1,l}(G^<_{l,l+1})$ indicates the matrix elements of the Hamiltonian (lesser Green's function) between the basis states in layer l +1 (l) and l (l +1) [12,40].

Before considering the e–ph interactions, let us briefly discuss the CMS approximation. The single-particle Hamiltonian in the EM approximation can be expressed as:

$$\begin{aligned}h(r)&=h_T+h_L\\&=\left[-\frac{\hbar^2}{2m^*_{y,z}}\Delta_{y,z}+V(r)\right]-\frac{\hbar^2}{2m^*_{y,z}}\frac{\partial^2}{\partial x^2}\end{aligned} \tag{10}$$

We can obtain the CMS representation by projecting each diagonal block $h_{n,n}$ of h_T on a subspace spanned by some chosen eigenmodes $\phi_i(y,z;n)$ of $h_{n,n}$ [41]. The transformation matrix is unitary in the limit where all the transverse modes are selected and, consequently, the CMS Hamiltonian is exactly equivalent to the real space Hamiltonian. On the other hand, the CMS Hamiltonian with few chosen modes is equal to the full rank EM Hamiltonian on the chosen subspace, as it reproduces by construction the exact selected EM sub-bands and their wavefunctions. Therefore, CMS offers the possibility to reproduce the effect of roughness or ionized impurities if enough modes are chosen. In this approximation, the matrix elements between the modes i and j read

$$\begin{aligned}&\tilde{G}^{R,\lessgtr}(l,i;l',j;E)=\\&\Sigma_{y,z}\Sigma_{y',z'}\phi_i^*(y,z;l)\cdot G^{R,\lessgtr}(l,y,z;l',y',z';E)\cdot\phi_j(y',z';l')\end{aligned} \tag{11}$$

To study the diffusive transport, the interactions of the electrons with phonons is implemented within the NESS via introducing the corresponding self-energies in real space [42,43]:

$$\Sigma^<_{\mathrm{ac},v}(r;E)=M_{\mathrm{ac}}G^<_v(r;E), \tag{12}$$

$$\Sigma^{<(>)}_{\mathrm{op},v}(r;E)=\Sigma_{q,v'}\left|M_q^{v,v'}\right|^2\left[n_{B,q}\cdot G^{<(>)}_{v'}\left(r;E-(+)\hbar\omega_q\right)+\left(n_{B,q}+1\right)\cdot G^{<(>)}_{v'}\left(r;E+(-)\hbar\omega_q\right)\right], \tag{13}$$

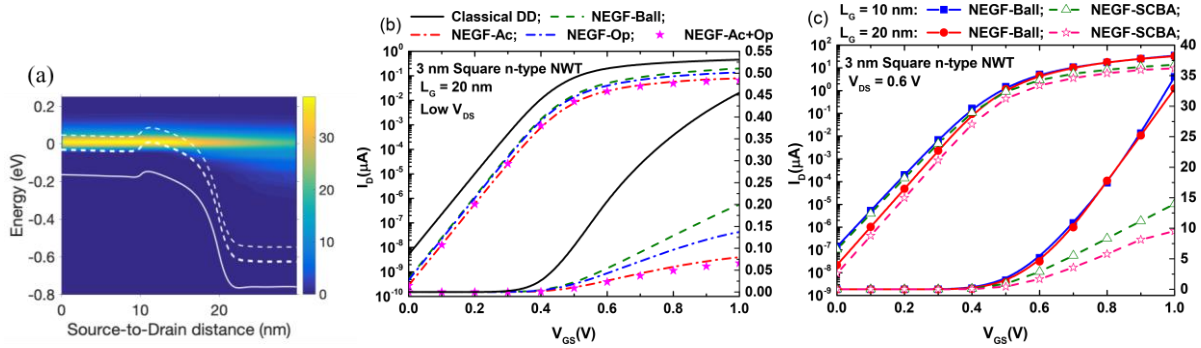

Figure 9. (a) The current spectrum in μA/eV for a NW with a square cross-section of 3nm×3nm and L_G=10nm calculated in the diffusive limit including e-ph scattering for ON-state (V_G=0.6V). The Fermi level at the source is the energy reference and V_{DS} = 0.6V. Moreover, the first subband of each valley is indicated with a white dashed line. The solid line corresponds to the potential along the transport direction which is the same as the first subband. I_{DS}–V_{GS} characteristics for n-type square 3nm×3nm Si NW assuming ballistic and dissipative NEGF transport simulations with: (b) L_G=20nm and low V_{DS} using the classical DD and the NEGF modules (including a combination of acoustic (Ac) and g-type optical (Op) phonon scattering mechanisms); and (c) L_G=10nm and L_G=20nm at V_{DS} = 0.6V.

where v, q, and $n_{B,q}$ refer to the electronic valley index, optical phonon with energy $\hbar\omega_q$, and the Bose-Einstein occupation number. The coupling constant of acoustic phonons M_{ac}, and the coupling strength of e–ph interaction $M_q^{v,v'}$ are obtained from the deformation potential theory [44]. The retarded component of the self-energy stemming from e-ph interactions may be expressed as:

$$\Sigma^{R}(r;E)=\frac{1}{2}\left[\Sigma^{>}(r;E)-\Sigma^{<}(r;E)\right]. \qquad (14)$$

Its CMS counterpart has the same form, whereas the real space self-energies are replaced by the CMS ones. Following the same notation as in Equation (11), and assuming that the self-energies are local in both space and time, the self-energies due to e-ph interactions in CMS representation read [45]:

$$\tilde{\Sigma}^{<}_{ac}(x,i;x,j;E)=M_{\mathrm{ac}}\sum_{k,l}F^{i,j}_{k,l}(x)\tilde{G}^{<}(x,k;x,l;E) \qquad (15)$$

$$\tilde{\Sigma}^{<(>)}_{op,v}(x,i;x,j;E)=\sum_{k,l}F^{i,j}_{k,l}(x)\sum_{q,v'}\left|M_q^{v,v'}\right|^2\left[\left(n_{B,q}+\frac{1}{2}\pm\frac{1}{2}\right)\tilde{G}^{<(>)}_{v'}\left(x,k;x,l;E\pm(\mp)\hbar\omega_q\right)\right]. \qquad (16)$$

We can define the total retarded (lesser) self-energy as $\Sigma^{R(<)}=\Sigma^{R(<)}_{C}+\Sigma^{R(<)}_{\mathrm{Scat}}$, where $\Sigma^{R(<)}$ refers to the impact of electron exchange with the contacts [14].

In Figure 9(a), we show the ON-state-current spectrum resulting from the simulations for a 3nm × 3nm square NW transistor including scattering processes at V_{DS} = 0.6V. The tunnelling current reaches high values up to 30 μA/eV. Overall current damping is observed due to acoustic phonons and energy relaxation of carriers as they approach the drain due to optical phonons emission. Figures 9(b) and (c) show the I_{DS}–V_{GS} characteristics for a n-type 3nm × 3nm square Si NW assuming ballistic and dissipative NEGF transport simulations. Figure 9(b) shows the results with L_G=20nm using the classical DD and the NEGF modules (Ac, g-type optical Op, and a combination of both phonon scattering mechanisms) at low drain voltage, whereas Figure 9(c) compares the results with L_G=10nm and L_G=20nm at V_{DS}=0.6V. More results from the NEGF module of NESS are presented in [1,14,15,16,18,20,22,39].

5. Conclusion

In this paper, we have described the organization and features of NESS - the new state-of-the-art device simulator from the Device Modeling Group at the University of Glasgow. We have highlighted the philosophy behind the project and demonstrated the capabilities of the various

modules that are ready for release as open-source software. NESS encompasses everything that is required for modern nanodevice simulation – a tool for structure generation, effective mass extractor, low-field mobility simulator, and a large array of carrier transport solvers – ranging from classical to semi-classical and quantum formalisms. There are several new modules under active development. We hope the device community will find NESS useful for advanced device research.

Acknowledgments

This project was initiated by the European Union Horizon 2020 research and innovation programme under grant agreement No. 688101 SUPERAID7 and has received further funding from EPSRC UKRI Innovation Fellowship scheme under grant agreement No. EP/S001131/1 (QSEE), No. EP/P009972/1 (QUANTDEVMOD) and No. EP/S000259/1(Variability PDK for design based research on FPGA/neuro computing); and from H2020-FETOPEN-2019 scheme under grant agreement No.862539-Electromed-FET OPEN. The coauthors would like to thank Dr. Carrillo-Nuñez, Dr. Lee, Dr. Berrada, Dr. Badami, and Dr. Duan for their former contribution to NESS; as well as Dr. Donetti for the possibility of using the 1DMC tool.

References

[1] O. Badami, C. Medina-Bailon, S. Berrada, *et al.*, "Comprehensive Study of Cross-Section Dependent Effective Masses for Silicon Based Gate-All-Around Transistors," *Applied Sciences* **9**(9), 1895, 2019.
[2] Synopsys inc, 2017, [online] Available: https://solvnet.synopsys.com/
[3] Silvaco, [online] Available: https://silvaco.com/
[4] S. Selberherr, "Simulation of Semiconductor Devices and Processes," *Springer-Verlag*, 1993.
[5] A. J. Garcia-Loureiro, N. Seoane, M. Aldegunde, *et al.*, "Implementation of the Density Gradient Quantum Corrections for 3-D Simulations of Multigate Nanoscaled Transistors," *IEEE Transactions on Computer-Aided Design of Integrated Circuits and Systems* **30**(6), 841-851, 2011.
[6] B. Winstead and U. Ravaioli, "A quantum correction based on Schrodinger equation applied to Monte Carlo device simulation," *IEEE Transactions on Electron Devices* **50**(2), 440-446, 2003.
[7] C. Riddet, A.R. Brown, C.L. Alexander, *et al.*, "3-D Monte Carlo Simulation of the Impact of Quantum Confinement Scattering on the Magnitude of Current Fluctuations in Double Gate MOSFETs," *IEEE Transactions on Nanotechnology* **6**, 48, 2007.
[8] N. Seoane, D. Nagy, G. Indalecio, *et.al.*, "A Multi-Method Simulation Toolbox to Study Performance and Variability of Nanowire FETs," *Materials* **12**(15), 2391, 2019.
[9] C. Medina-Bailon, J.L. Padilla, T. Sadi, *et al.*, " Multisubband ensemble Monte Carlo analysis of tunneling leakage mechanisms in ultrascaled FDSOI, DGSOI, and FinFET devices," *IEEE Trans. Electron Devices* **66**(3), 1145-1152, 2019.
[10] L. Donetti, C. Sampedro, F.G. Ruiz, *et al.*, "Multi-Subband Ensemble Monte Carlo simulations of scaled GAA MOSFETs," *Solid-State Electronics* **143**, 49-55, 2018.
[11] S. Jin, T.-W. Tang, and M. V. Fischetti, "Simulation of Silicon Nanowire Transistors Using Boltzmann Transport Equation Under Relaxation Time Approximation," *IEEE Trans. Electron Devices* **55**(3), 727-736, 2008.
[12] A. Svizhenko, M. P. Anantram, T. R. Govindan, *et al.*, "Two-dimensional quantum mechanical modeling of nanotransistors," *Journal of Applied Physics* **91**, 2343, 2002.
[13] M. Luisier and G. Klimeck, "Atomistic full-band simulations of silicon nanowire transistors Effects of electron-phonon scattering," *Phys Rev B* **80**, 155430, 2009.
[14] S. Berrada, H. Carrillo-Nuñez, J. Lee, *et al.*, "Nano-Electronic Simulation Software (NESS): a flexible nano-device simulation platform," *Journal of Computational Electronics* **19**, 1031–1046, 2020.
[15] J. Lee, O. Badami, H. Carrillo-Nuñez, *et al.*, "Variability Predictions for the Next Technology Generations of n-type SixGe1-x Nanowire MOSFETs," *Micromachines* **9**(12), 643, 2018.
[16] J. Lee, S. Berrada, H. Carrillo-Nuñez, *et al.*, "The Impact of Dopant Diffusion on Random Dopant Fluctuation in Si Nanowire FETs: A Quantum Transport Study," *2018 International Conference on Simulation of Semiconductor Processes and Devices (SISPAD)*, 280-283, 2018.
[17] T. Dutta, C. Medina-Bailon, H. Carrillo-Nuñez, *et al.*, "Schrödinger Equation Based Quantum Corrections in Drift-Diffusion: A Multiscale Approach," *IEEE Nanotechnology Materials and Devices Conference (NMDC)*, 2019.
[18] C. Medina-Bailon, O. Badami, H. Carrillo-Nuñez, *et al.*, "Enhanced Capabilities of the Nano-Electronic Simulation Software (NESS)," *2020 International Conference on Simulation of Semiconductor Processes and Devices (SISPAD)*, September 2020.
[19] T. Sadi, C. Medina-Bailon, M. Nedjalkov, *et al.*, "Simulation of the Impact of Ionized Impurity Scattering on the Total Mobility in Si Nanowire Transistors," *Materials* **12**(1), 124, 2019.
[20] O. Badami, S. Berrada, H. Carrillo-Nuñez, *et al.*, "Surface Roughness Scattering in NEGF using self-energy formulation," *2019 International Conference on Simulation of Semiconductor Processes and Devices (SISPAD)*, 2019.
[21] O. Badami, T. Sadi, F. Adamu-Lema, *et al.*, "A Kinetic Monte Carlo study of retention time in a POM molecule-based flash memory," *IEEE Transactions on Nanotechnology*, Early Access, 2020.
[22] H. Carrillo-Nuñez, C. Medina-Bailon, V.P. Georgiev, *et al.*, "Full-band quantum transport simulation in presence

of hole-phonon interactions using a mode-space k·p approach," *Nanotechnology Journal*, Early Access, 2020.
[23] A. Asenov, "Random dopant induced threshold voltage lowering and fluctuations in sub-0.1 μm MOSFETs: A 3D "atomistic" simulation study," *IEEE Trans. Electron Devices* **45**(12), 2505–2513, 1998.
[24] S. Kaya, A.R. Brown, A. Asenov, *et al.*, "Analysis of Statistical Fluctuations due to Line Edge Roughness in sub-0.1μm MOSFETs," *Simulation of Semiconductor Processes and Devices*, Springer, 2001.
[25] A. Brown, J. Watling and A. Asenov, "Intrinsic parameter fluctuations due to random grain orientations in high-k gate stacks," *J. Comput. Electron.* **5**(4), 333-336, 2006
[26] D. L. Scharfetter and D. L. Gummel, "Large signal analysis of a Silicon Read diode oscillator," *IEEE Trans. Electron Devices*, **16**, 64-77, 1969.
[27] G. Masetti, M. Severi, and S. Solmi, "Modeling of carrier mobility against carrier concentration in Arsenic-, Phosphorus-, and Boron-doped Silicon," *IEEE Trans. Electron Devices* **30**(7), 764–769, 1983.
[28] K. Yamaguchi, "Field-dependent mobility model for two-dimensional numerical analysis of MOSFET's," *IEEE Trans. Electron Devices* **26**(7), 1068–1074, 1979.
[29] D. Caughey and R. Thomas, "Carrier mobilities in silicon empirically related to doping and field," *Proceedings of the IEEE* **55**(12), 2192–2193, 1967.
[30] G. Fiori and G. Iannaccone, "Three-dimensional simulation of one-dimensional transport in silicon nanowire transistors," *IEEE Transactions on Nanotechnology* **6**(5), 524–529, 2007.
[31] G.A. Kathawala and U. Ravaioli, "3-D monte-carlo simulations of FinFETs," *IEEE International Electron Devices Meeting (IEDM)*, 29–2, 2003.
[32] A. R. Brown, J. R. Watling, G. Roy, *et al.*, "Use of density gradient quantum corrections in the simulation of statistical variability in MOSFETs," *Journal of Computational Electronics* **9**(3-4), 187–196, 2010.
[33] C. Medina-Bailon, T. Sadi, M. Nedjalkov, *et al.*, "Study of the 1D Scattering Mechanisms' Impact on the Mobility in Si Nanowire Transistors," *2018 Joint International EUROSOI Workshop and International Conference on Ultimate Integration on Silicon (EUROSOI-ULIS)*, 2018.
[34] C. Medina-Bailon, T. Sadi, M. Nedjalkov, *et al.*, "Impact of the Effective Mass on the Mobility in Si Nanowire Transistors," *2018 International Conference on Simulation of Semiconductor Processes and Devices (SISPAD)*, 297-300, 2018.
[35] L. V. Keldysh, "Diagram Technique for Nonequilibrium Processes," *Sov. Phys. JETP* **20**(4), 1018, 1965.
[36] G. D. Mahan, "Many-Particle Physics, Physics of Solids and Liquids," *Springer*, 2000.
[37] G. Stefanucci and R. Van Leeuwen, "Nonequilibrium Many-Body Theory of Quantum Systems: A Modern Introduction, " *Cambridge University Press*, 2013.
[38] C. Medina-Bailon, H. Carrillo-Nuñez, J. Lee, *et al.*, "Quantum Enhancement of a S/D Tunneling Model in a 2D MS-EMC Nanodevice Simulator: NEGF Comparison and Impact of Effective Mass Variation," *Micromachines* **11**(2), 204, 2020.
[39] H. Carrillo-Nuñez, J. Lee, S. Berrada, *et al.*, "Random Dopant-Induced Variability in Si-InAs Nanowire Tunnel FETs: A Quantum Transport Simulation Study", *IEEE Electron Device Lett*. **39**(9), 1473-1476, 2018.
[40] M. P. Anantram, "Modeling of nanoscale devices, " *Proc. IEEE* 96, 1511–1550, 2008.
[41] M. Luisier, A. Schenk, W. Fichtner, "Quantum transport in two- and three-dimensional nanoscale transistors: coupled mode effects in the nonequilibrium Green's function formalism, " *J. Appl. Phys.* **100**(4), 043713, 2006.
[42] M. Aldegunde, A. Martinez, A. Asenov, "Non-equilibrium Green's function analysis of cross section and channel length dependence of phonon scattering and its impact on the performance of Si nanowire field effect transistors, " *J. Appl. Phys.* **110**(9), 094518, 2011.
[43] M. Bescond, C. Li, H. Mera, et al., "Modeling of phonon scattering in n-type nanowire transistors using one-shot analytic continuation technique, " *J. Appl. Phys.* **114**(15), 153712, 2013.
[44] C. Jacoboni, L. Reggiani, "The Monte Carlo method for the solution of charge transport in semiconductors with applications to covalent materials," *Rev. Mod. Phys.* **55**, 645–705, 1983.
[45] A. Esposito, F. Martin, A. Schenk, "Quantum transport including nonparabolicity and phonon scattering: application to silicon nanowires," *J. Comput. Electron.* **8**(3), 336, 2009.

Photography & Biography

Cristina Medina-Bailon received the Ph.D. in Electronics from the Univ. of Granada, Spain, in 2017. Her current research interests focus on the Monte Carlo description of tunneling phenomena and on the implementation of classical and semi-classical approaches. In July 2017, she joined the Device Modelling Group at the University of Glasgow as Post-doctoral fellow and she is the software coordinator of NESS since March 2019.

Tapas Dutta received the Ph.D. degree in nanoelectronics and nanotechnology from the Grenoble INP, France in 2014. He was with IIT Kanpur, India as a postdoctoral researcher during 2014-17. Since September 2017, he has been with the Device Modeling Group at the University of Glasgow, where he has been a co-developer of NESS. His research interests are TCAD software development, and compact modeling of emerging electronic devices.

Fikru Adamu-Lema received the Ph.D. degree in electronics engineering from the University of Glasgow in 2006. He then joined Visual Numerics International, Ltd., (now a part of Rogue Wave software) as a Technical Engineer for IMSL numerical algorithms. He is currently an RA with the Device Modelling Group at the University of Glasgow and Semiwise Ltd. His current research interests include the development of reliability models, and statistical simulation study of nanoscale MOSFETs and SRAM circuit simulations.

Ali Rezaei received his Ph.D. (Dr. rer. nat.) in Condensed Matter Physics at the University of Konstanz, Konstanz, Germany, in 2019. In August 2020, he joined the Device Modelling Group, School of Engineering at the University of Glasgow as a Postdoctoral Research Associate to focus primarily on the further development and expanding the functionality of the non-equilibrium Green's function (NEGF) quantum transport module of NESS.

Daniel Nagy received the M.Res. degree in nanoscience to nanotechnology and the Ph.D. degree in electronic and electrical engineering from Swansea University, Swansea, U.K., in 2013 and 2016, respectively. He held a Post-Doctoral position between 2016 and 2019 at the CITIUS, University of Santiago de Compostela, Santiago de Compostela, Spain. He joined the Device Modelling Group, School of Engineering, University of Glasgow, where he is a Research Associate since 2020 April.

Vihar P. Georgiev received his Ph.D. degree from the University of Oxford, Oxford, U.K., in 2011. In 2011, he joined the Device Modelling Group, School of Engineering, University of Glasgow, where he was a Research Associate until 2015 and currently he is a Senior Lecturer in electronics and nanoscale engineering. He is also UKRI EPSRC innovation fellow.

Asen Asenov (M'96–SM'05–F'11) received the Ph.D. degree in solid-state physics from the Bulgarian Academy of Sciences, Sofia, Bulgaria, in 1989. He was a Chief Executive Officer with Gold Standard Simulations, Ltd., Glasgow, U.K. Currently, he is a James Watt Professor of Electrical Engineering with the University of Glasgow.